Turkish Journal of Electrical Engineering & Computer Sciences

http://journals.tubitak.gov.tr/elektrik/

Research Article

Turk J Elec Eng & Comp Sci
(2017) 25: 995 – 1009

doi:10.3906/elk-1506-250

Modeling and analysis of a novel dual open-end stator windings wound rotor synchronous machine with dampers

Abdelmonoem NAYLI[1,2,*], **Sami GUIZANI**[2,3], **Faouzi BEN AMMAR**[2]
[1]University of Tunis, ENSIT, Tunisia
[2]University of Carthage, MMA Laboratory, INSAT, Tunisia
[3]University of El Manar, IPEIEM, Tunisia

Received: 28.06.2015 • **Accepted/Published Online:** 15.03.2016 • **Final Version:** 10.04.2017

Abstract: This work presents a novel wound rotor synchronous machine with dampers with dual three-phase open-end stator windings. The aim of the proposed machine is to improve the power segmentation and the availability of the drive system. The mathematical model of this machine is presented in the Park reference frame. This machine is supplied by four 2-level inverters, where each inverter is dimensioned for quarter power of the machine. For comparison purposes, we use a double star synchronous machine fed by two 2-level inverters. Comparative simulation analysis using THD voltage, THD stator current, and torque undulation showed significant advantages of the proposed machine.

Key words: Dual open-end stator windings synchronous machine, double star synchronous machine, power segmentation, availability

1. Introduction

Synchronous machines are widely used in industry, particularly permanent magnet synchronous machines. These machines are essentially present for low and medium power. For high power, wound rotor synchronous machines are mainly used in the field of production of electrical energy [1]. Obviously, the association of the converters with these machines remains a problem because of the cutting frequency limitation. Several searches were carried out at levels of the converter in order to remedy this problem using multilevel inverters with topology NPC, flying-capacitor, and cascaded H-bridge inverter [2–6]. Other research has presented solutions at the levels of the stator windings structures such as multiphase machines and multistar machines [7–15]. In recent years, the open-end winding machine, which is proposed by Stemmler and Geggenbach [16], is presented in [17–20]. Next, the multiphase open-end winding machine structure with five-phase open-end winding configuration is presented in [21]. Furthermore, new publications have presented a novel machine structure, which is a three-phase dual open-end winding induction machine fed by four voltage source inverters [22,23]. This machine offers power segmentation and improves the reliability and availability of the drive system. In particular, it increases the liberty degrees in degraded mode.

Then the authors present a novel structure of dual open-end stator windings synchronous machine "DOEWSM" with salient-pole wound rotor with damper windings. Such a stator windings structure is shown in Figure 1.

*Correspondence: n.ayli@hotmail.fr

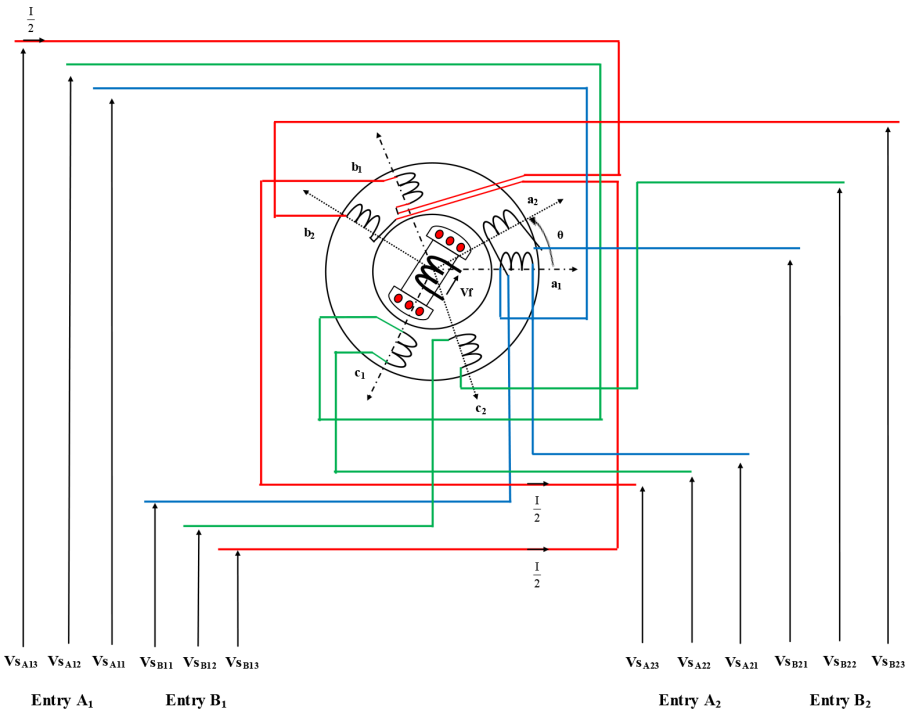

Figure 1. Voltage supply of the dual three-phase open-end windings synchronous machine "DOEWSM".

In the first part, the modelling of the dual three-phase open-end stator windings synchronous machine with damper windings is presented in Park (d, q) reference frame. The simulation model of the machine for voltage supply is implemented in MATLAB Simulink environment.

In the second part, the feeding of the machine by four three-phase 2-level inverters based on PWM control strategy is presented. The different obtained results of the THD voltage, THD stator current, and torque undulation are compared with the double star synchronous machine "DSSM". Finally, the influence of damper windings for "DOEWSM" is shown by the simulation results of speed and torque.

2. Modelling of the dual open-end windings wound rotor synchronous machine with dampers in Park reference frame

Park transformation allows reproduction of the magnetic state created by the three-phase system by means of an equivalent two-phase system. Indeed, three-phase stator magnitudes shifted of 120° (S11, S12, S13) and (S21, S22, S23) as shown in Figure 2 are brought to the two-phase magnitudes in the reference frame of Park (d, q) rotating at the speed ωr, which allows removal of the no-linearity. The winding rotor is not transformed. Figure 3 represents the model of the wound rotor synchronous machine with damper windings in the (d, q) reference frame.

The developed model is based on the following assumptions:

- The stator windings m.m.f. is in sinusoidal space distribution.
- The saturation of the magnetic circuit, the hysteresis, and the eddy currents are neglected.
- The skin effect that increases resistances and decreases inductances is neglected.

The flux equations in matrix form on the axis (d, q):

$$[\psi] = [L]\,[I] \tag{1}$$

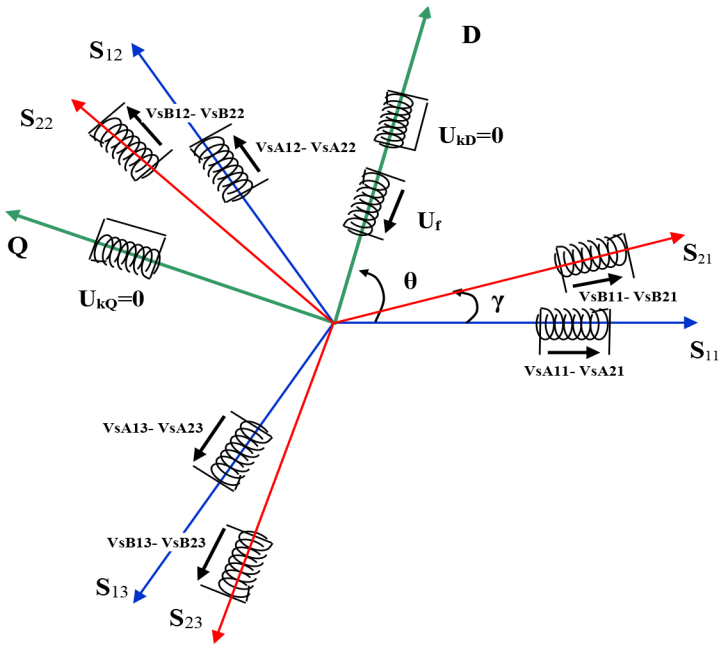

Figure 2. Three-phase system of the dual three-phase open-end windings synchronous machine with damper windings.

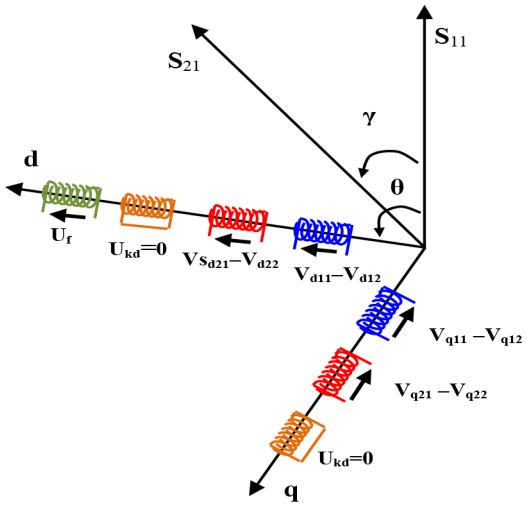

Figure 3. Representation of the machine in the (d, q) reference frame.

The voltage equations in the reference frame (d, q) are

$$[V] = [R]\,[I] + \frac{d}{dt}\,[\psi] + [\omega]\,[\psi] \tag{2}$$

with

$$[V] = \left[\begin{array}{cccccccc} V_{sd11} - V_{sd12} & V_{sd21} - V_{sd22} & V_{sq11} - V_{sq12} & V_{sq21} - V_{sq22} & V_f & 0 & 0 \end{array}\right]^T$$

$$[I] = \left[\begin{array}{ccccccc} i_{sd1} & i_{sd2} & i_{sq1} & i_{sq2} & i_f & i_{kd} & i_{kq} \end{array}\right]^T$$

$$[\psi] = \left[\begin{array}{ccccccc} \psi_{sd1} & \psi_{sd2} & \psi_{sq1} & \psi_{sq2} & \psi_f & \psi_{kd} & \psi_{kq} \end{array}\right]^T$$

$$[L] = \begin{bmatrix} L_d & M_d & 0 & 0 & M_{fd} & M_{kd} & 0 \\ M_d & L_d & 0 & 0 & M_{fd} & M_{kd} & 0 \\ 0 & 0 & Lq & M_q & 0 & 0 & M_{kq} \\ 0 & 0 & M_q & L_d & 0 & 0 & M_{kq} \\ M_{fd} & M_{fd} & 0 & 0 & L_f & M_{fkd} & 0 \\ M_{kd} & M_{kd} & 0 & 0 & Mf_{kd} & L_{kd} & 0 \\ 0 & 0 & M_{kq} & M_{kq} & 0 & 0 & L_{kq} \end{bmatrix} \tag{3}$$

$$[R] = \begin{bmatrix} R_s & 0 & 0 & 0 & 0 & 0 & 0 \\ 0 & R_s & 0 & 0 & 0 & 0 & 0 \\ 0 & 0 & R_s & 0 & 0 & 0 & 0 \\ 0 & 0 & 0 & R_s & 0 & 0 & 0 \\ 0 & 0 & 0 & 0 & R_f & 0 & 0 \\ 0 & 0 & 0 & 0 & 0 & R_{kd} & 0 \\ 0 & 0 & 0 & 0 & 0 & 0 & R_{kq} \end{bmatrix} \tag{4}$$

$$[\omega] = \begin{bmatrix} 0 & 0 & -\omega_r & 0 & 0 & 0 & 0 \\ 0 & 0 & 0 & -\omega_r & 0 & 0 & 0 \\ \omega_r & 0 & 0 & 0 & 0 & 0 & 0 \\ 0 & \omega_r & 0 & 0 & 0 & 0 & 0 \\ 0 & 0 & 0 & 0 & 0 & 0 & 0 \\ 0 & 0 & 0 & 0 & 0 & 0 & 0 \\ 0 & 0 & 0 & 0 & 0 & 0 & 0 \end{bmatrix}, \tag{5}$$

where R_s is the resistance of the stator, R_f is the resistances of the excitation winding of rotor, R_{kd} and R_{kq} are the resistance of damper winding, and d- and q-axis, respectively. L_d and L_q are the inductance of the stator, and d- and q-axis, respectively. L_f is the inductance of the excitation winding of the rotor. M_d and M_q are the mutual inductance of the stator, and d- and q-axis, respectively. M_{fd} is the mutual inductance between stator d_1, $_2$-axis and excitation winding of the rotor. M_{fkd} is the mutual inductance between damper winding and excitation winding of the rotor. M_{kd} is the mutual inductance between stator d_1, $_2$-axis and dampers winding of the rotor. M_{kq} is the mutual inductance between stator $q_{1,2}$-axis and dampers winding of the rotor. M_q is the mutual inductance between stator q_1-axis and stator q_2-axis.

3. Simulation model of the "DOEWSM"

If the "DOEWSM" is supplied by four voltage sources, the mathematical current model is written in (d, q) reference frame ($\omega_r = \omega_{dq}$), and described by the following state equation representation:

$$\begin{cases} \frac{dX(t)}{dt} = [A(\omega, \omega_{dq}] \ [X(t)] + [B].U(t) \\ Y(t) = [C] \ X(t) \end{cases} \tag{6}$$

with

$X(t) = \left[\begin{array}{cccccc} i_{sd1} & i_{sd2} & i_{sq1} & i_{sq2} & i_f & i_{kd} & i_{kq} \end{array} \right]^T$: State vector

$U(t) = \left[\begin{array}{cccccccc} V_{sd11} - V_{sd12} & V_{sd21} - V_{sd22} & V_{sq11} - V_{sq12} & V_{sq21} - V_{sq22} & V_f & 0 & 0 \end{array} \right]^T$: Control vector

$Y(t) = \left[\begin{array}{cccccc} \psi_{sd1} & \psi_{sd2} & \psi_{sq1} & \psi_{sq2} & \psi_f & \psi_{kd} & \psi_{kq} \end{array} \right]^T$: Output vector

The functional diagram is given in Figure 4.

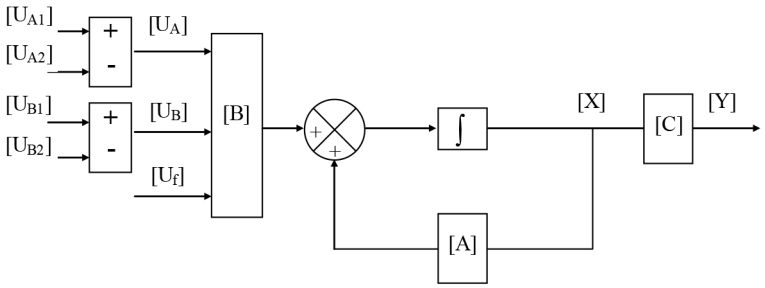

Figure 4. Functional diagram of the synchronous machine "DOEWSM".

The state matrix $[A]$ is

$$\frac{d}{dt}[I] = [A].[I] + [B][V] \tag{7}$$

with

$$[A] = -([R].[L]^{-1} + [\omega]) \tag{8}$$

The matrix $[B]$ is

$$[B] = [L]^{-1} \tag{9}$$

The matrix $[C]$ is

$$[C] = [L] \tag{10}$$

with

$$[A] = -\begin{bmatrix} R_sK_1 & R_sK_2 & -\omega_r & 0 & \frac{R_s(L_{kd}M_{fd}-M_{fkd}M_{kd})}{X_1} & \frac{R_s(L_fM_{kd}-M_{fd}M_{fkd})}{X_1} & 0 \\ R_sK_2 & R_sK_1 & 0 & -\omega_r & \frac{R_s(L_{kd}M_{fd}-M_{fkd}M_{kd})}{X_1} & \frac{R_s(L_fM_{kd}-M_{fd}M_{fkd})}{X_1} & 0 \\ \omega_r & 0 & \frac{R_s(L_{kq}L_q-M_{kq}^2)}{X_2(L_q-M_q)} & \frac{R_s(M_{kq}^2-L_{kq}M_q)}{X_2(L_q-M_q)} & 0 & 0 & \frac{-M_{kq}}{X_2} \\ 0 & \omega_r & \frac{R_s(M_{kq}^2-L_{kq}M_q)}{X_2(L_q-M_q)} & \frac{R_s(L_{kq}L_q-M_{kq}^2)}{X_2(L_q-M_q)} & 0 & 0 & \frac{-M_{kq}}{X_2} \\ R_fK_3 & R_fK_3 & 0 & 0 & \frac{R_f(2M_{fd}M_{kd}-L_{kd}(L_d+M_d))}{X_1} & \frac{R_f(M_{fkd}(L_d+M_d)-2M_{fd}M_{kd}))}{X_1} & 0 \\ R_{kd}K_4 & R_{kd}K_4 & 0 & 0 & \frac{R_{kd}((L_d+M_d)M_{fkd}-2M_{fd}^2)}{X_1} & \frac{R_{kd}(2M_{fd}^2-L_f(L_d+M_d))}{X_1} & 0 \\ 0 & 0 & \frac{-R_{kq}M_{kq}}{X_2} & \frac{-R_{kq}M_{kq}}{X_2} & 0 & 0 & \frac{R_{kq}(L_q+M_q)}{X_2} \end{bmatrix}$$

$$[L]^{-1} = \begin{bmatrix} K_1 & K_2 & 0 & 0 & \frac{L_{kd}M_{fd}-M_{fkd}M_{kd}}{X_1} & \frac{L_fM_{kd}-M_{fd}M_{fkd}}{X_1} & 0 \\ K_2 & K_1 & 0 & 0 & \frac{L_{kd}M_{fd}-M_{fkd}M_{kd}}{X_1} & \frac{L_fM_{kd}-M_{fd}M_{fkd}}{X_1} & 0 \\ 0 & 0 & \frac{(L_{kq}L_q-M_{kq}^2)}{X_2(L_q-M_q)} & \frac{(M_{kq}^2-L_{kq}M_q)}{X_2(L_q-M_q)} & 0 & 0 & \frac{-M_{kq}}{X_2} \\ 0 & 0 & \frac{(M_{kq}^2-L_{kq}M_q)}{X_2(L_q-M_q)} & \frac{(L_{kq}L_q-M_{kq}^2)}{X_2(L_q-M_q)} & 0 & 0 & \frac{-M_{kq}}{X_2} \\ K_3 & K_3 & 0 & 0 & \frac{2M_{fd}M_{kd}-L_{kd}(L_d+M_d)}{X_1} & \frac{M_{fkd}(L_d+M_d)-2M_{fd}M_{kd})}{X_1} & 0 \\ K_4 & K_4 & 0 & 0 & \frac{(L_d+M_d)M_{fkd}-2M_{fd}^2}{X_1} & \frac{2M_{fd}^2-L_f(L_d+M_d)}{X_1} & 0 \\ 0 & 0 & \frac{-M_{kq}}{X_2} & \frac{-M_{kq}}{X_2} & 0 & 0 & \frac{(L_q+M_q)}{X_2} \end{bmatrix}$$

$$X_1 = 2M_{fd}^2(L_{kd} - M_{fkd}) + M_{fkd}^2(L_d + M_d) + 2M_{fd}M_{kd}(L_f - M_{fkd}) - L_f(L_{kd}M_d + L_dL_{kd})$$

$$X_2 = -2M_{kq}^2 + L_{kq}(L_q + M_q)$$

$$K_1 = -\frac{L_d(L_fL_{kd} - M_{fkd}^2) + M_{fd}((M_{fkd} - L_{kd})M_{fd} + (M_{fkd} - L_f)M_{kd})}{X_1.(L_d - M_d)}$$

$$K_2 = -\frac{(L_{kd}M_{fd}^2 + M_{fkd}(-M_{fd}^2 + M_dM_{fkd} - M_{fd}M_{kd}) + L_f(-L_{kd}M_d + M_{fd}M_{kd}))}{X_1.(L_d - M_d)}$$

$$K_3 = \frac{M_{fd}(L_{kd} - M_{fkd})}{X_1};$$

$$K_4 = \frac{M_{fd}(L_f - M_{fkd})}{X_1};$$

The mechanical equation is given by the following relationship:

$$T_{em} - T_r = j\frac{d\omega}{dt} + f\omega \tag{11}$$

The general expression of the electromagnetic torque is

$$\begin{aligned} T_{em} = {} & \tfrac{3}{2}p((L_d - L_q)(i_{sd1}i_{sq1} + i_{sd2}i_{sq2}) + (M_d - M_q)(i_{sd2}i_{sq1} + i_{sd1}i_{sq2}) \\ & + (i_{sq1} + i_{sq2})(M_{fd}i_f + M_{kd}i_{kd}) - M_{kq}i_{kq}(i_{sd1} + i_{sd2})) \end{aligned} \tag{12}$$

4. Supply of the machine by three-phase 2-level inverters

The simulation model of the proposed machine is validated in MATLAB Simulink environment. Each entry of stator winding is supplied by a three-phase 2-level inverter, as shown in Figure 5. We used carrier PWM for control inverters. The strategy PWM involves the use of six reference voltages of frequency fs = 50 Hz; the three reference voltages (Vs_{11}, Vs_{12}, and Vs_{13}) are shifted by 120° between them, also three other (Vs_{21}, Vs_{22} and Vs_{23}) are shifted by 120° between them, but the last three are shifted from to the first reference voltages by an angle of 180°. These reference voltages are compared with carrier frequency fp for control the switching of devices in each inverter, as shown in Figure 6.

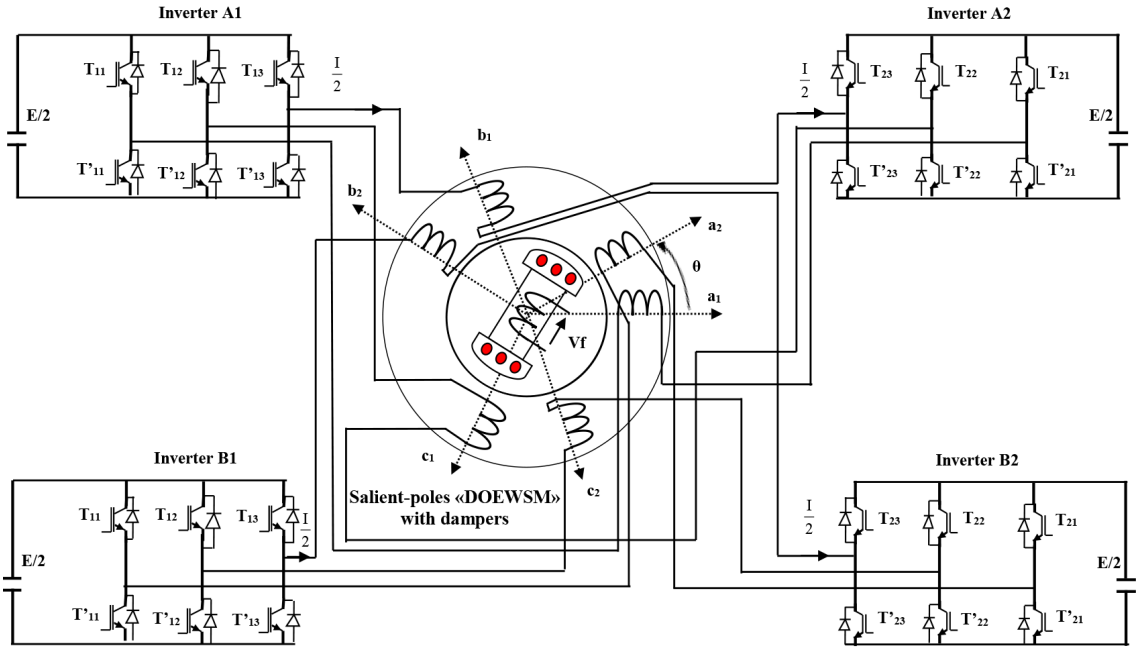

Figure 5. Supply "DOEWSM" by four three-phase 2-level inverters.

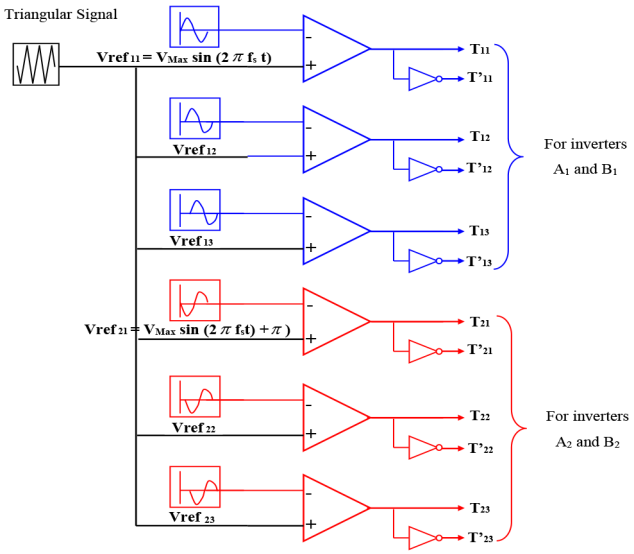

Figure 6. Principle of the PWM sine triangle.

The reference voltage signals with carrier triangular for control inverters to supply the machine are shown in Figure 7.

Figure 8 shows the voltage (Vs_{11}–Vs_{12}), (Vs_{21}–Vs_{22}) and phase-to-phase voltage (U_A) of stator windings A, which is 3 levels to supply with two three-level inverters, the same simulation results for the voltages of stator winding B. We used carrier PWM for control inverters with carrier frequency fp = 5000 Hz,

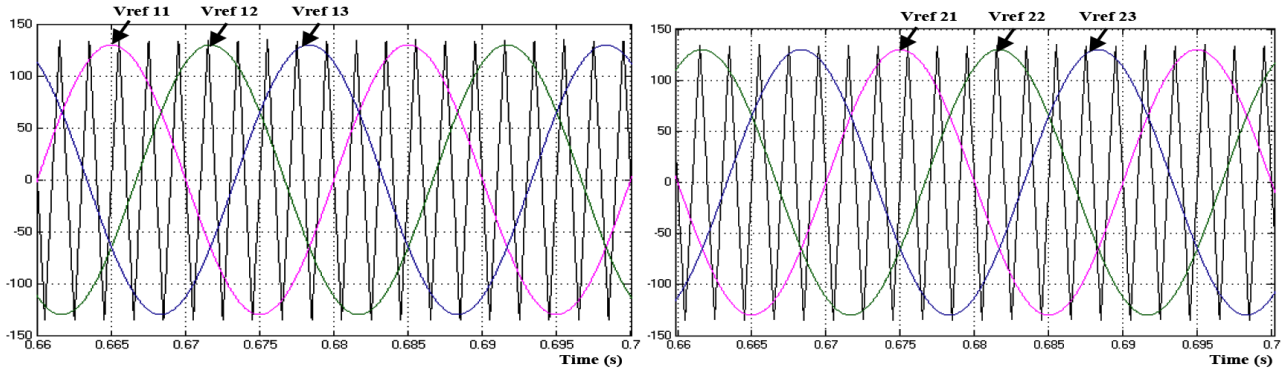

Figure 7. Reference voltages with a triangular signal for control inverters.

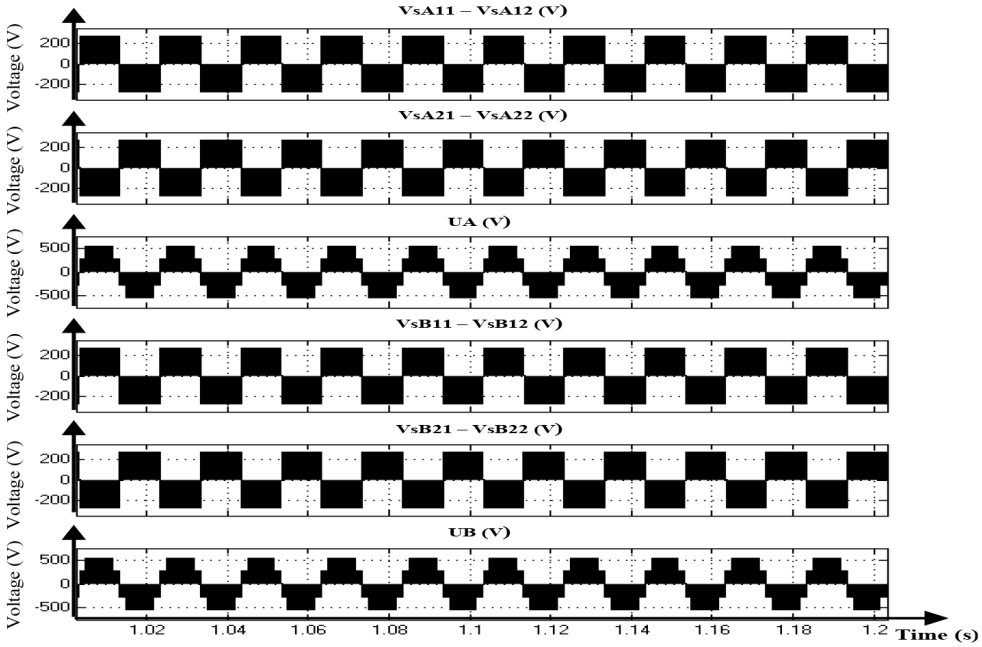

Figure 8. Pole voltage inverters and phase-to-phase machine voltage.

with

Vs_{A11}, Vs_{A12}, and Vs_{A13}: simple voltage of inverter A_1

Vs_{A21}, Vs_{A22}, and Vs_{A23}: simple voltage of inverter A_2

Vs_{B11}, Vs_{B12}, and Vs_{B13}: simple voltage of inverter B_1

Vs_{B21}, Vs_{B22}, and Vs_{B23}: simple voltage of inverter B_2

(Vs_{A11}–Vs_{A12}): pole voltage of inverter A_1

(Vs_{A21}–Vs_{A22}): pole voltage of inverter A_2

(Vs_{B11}–Vs_{B12}): pole voltage of inverter B_1

(Vs_{B21}–Vs_{B22}): pole voltage of inverter B_2

$U_A = (Vs_{A11}–Vs_{A12})–(Vs_{A21}–Vs_{A22})$: phase-to-phase voltage of stator winding A

$U_B = (Vs_{B11}–Vs_{B12})–(Vs_{B21}–Vs_{B22})$: phase-to-phase of stator winding B.

We also modeled and simulated the double star synchronous machine " DSSM " with damper winding to compare with the proposed machine. The evolution of the currents, speed, and torque T_{em} for the two machines for the power P = 40 kW is shown in Figure 9. At t = 0 s to t = 1 s, the system has a starting cycle

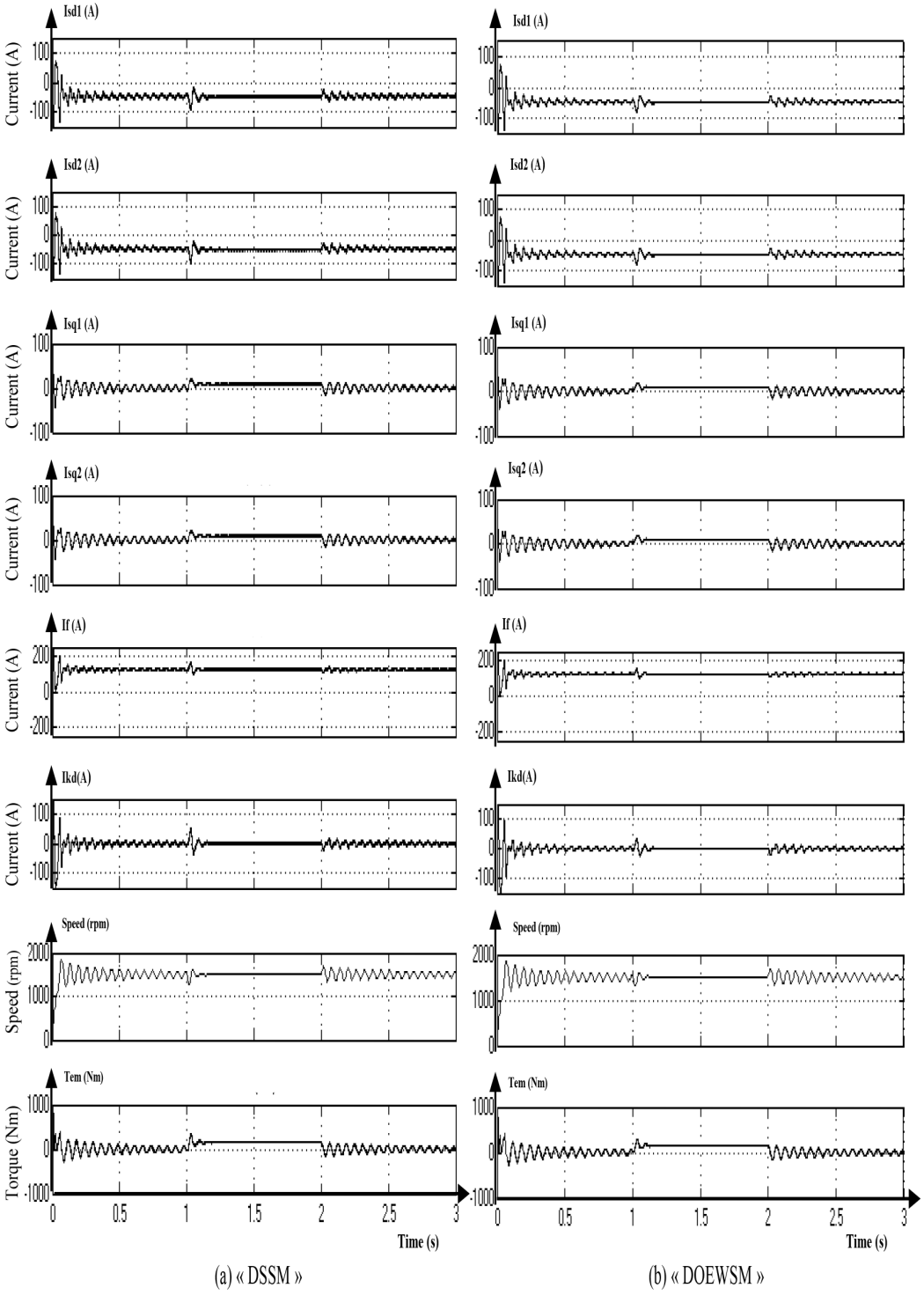

Figure 9. Evolution of the currents, speed, and torque.

in which the machine is working in no-load condition. At time t = 1 s, the impact of torque Tr = 150 Nm is applied. At time t = 2s, the no-load torque is applied.

Figure 10 shows the waveform and the harmonic content of the phase-to-phase machine voltage with THD voltage = 70.06% of the machine "DSSM" and THD voltage = 44.05% of the machine "DOEWSM".

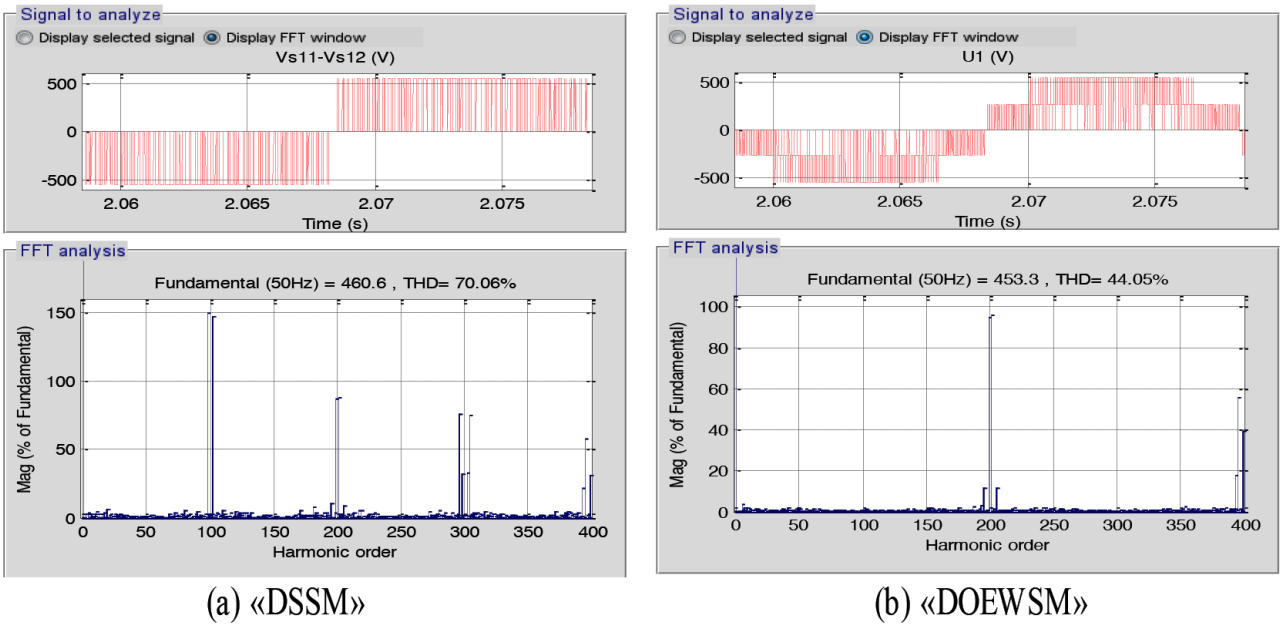

Figure 10. Waveform and harmonic ration of machine voltage.

We notice that the machine "DOEWSM" offers extended band-width, increased level of voltage, and better THD voltage.

In order to analyze the torque undulations, we defined ΔTem by the expression

$$\Delta Tem = \frac{T_{Max} - T_{moy}}{T_{moy}} 100 \tag{13}$$

Figure 11 shows the enlarging effect of the torque during the permanent mode for a load torque Tr = 150 Nm.

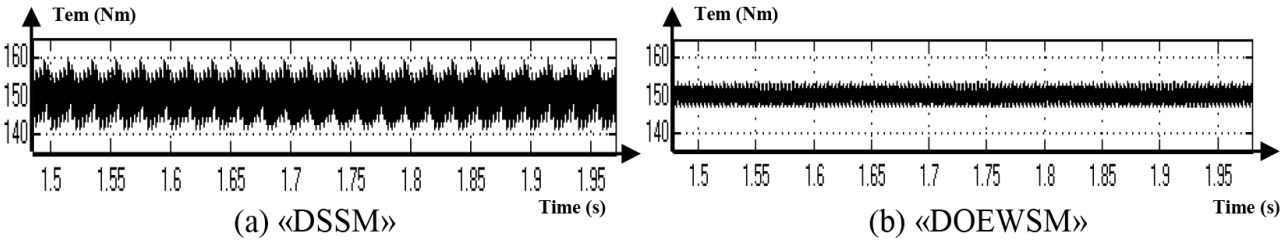

Figure 11. Enlarging effect of the waveform torque.

The calculation of the undulation torque in a permanent regime is

For the machine "DSSM": $\Delta Tem = \frac{157.2-150}{150} 100 = 4.8\,\%$

For the machine "DOEWSM": $\Delta Tem = \frac{152.7-150}{150}100 = 1.8\,\%$

The machine "DOEWSM" gives a better quality of the torque.

The simulation results of stator current of the two machine structures "DSSM" and "DOEWSM" during the starting and permanent mode are shown in Figure 12.

The zoom of evolution of stator current of the two machines in permanent mode is given in Figure 13.

Figure 14 shows the waveform and the harmonic content of the stator current with THD current = 2.27% of the machine "DSSM" and THD current = 0.65% of the machine "DOEWSM".

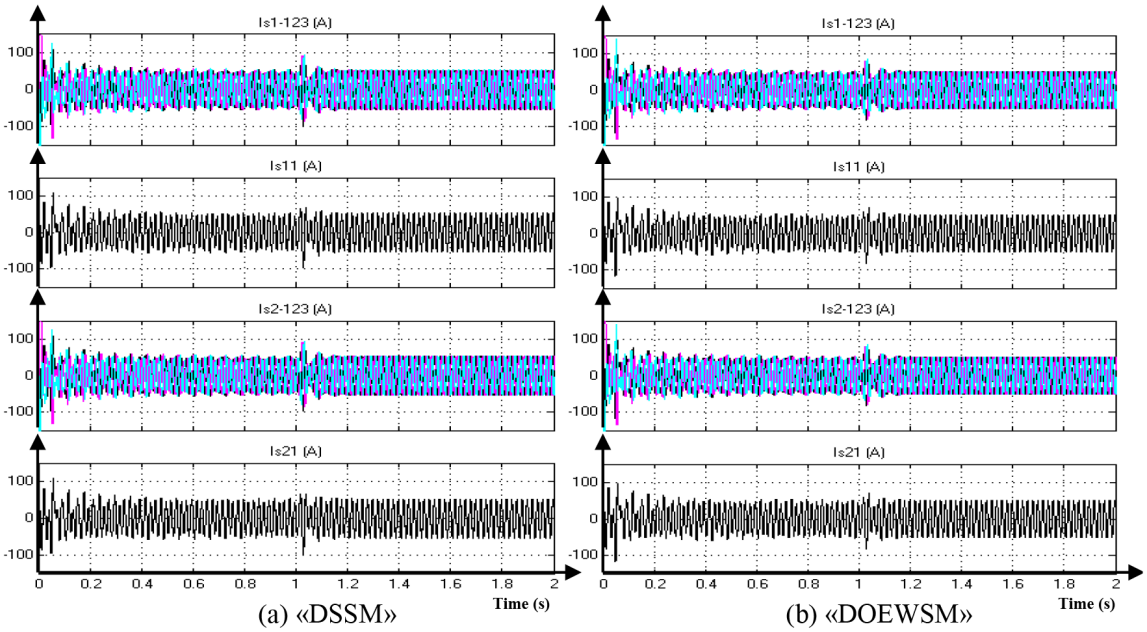

Figure 12. Evolution of the stator currents during the starting and permanent mode.

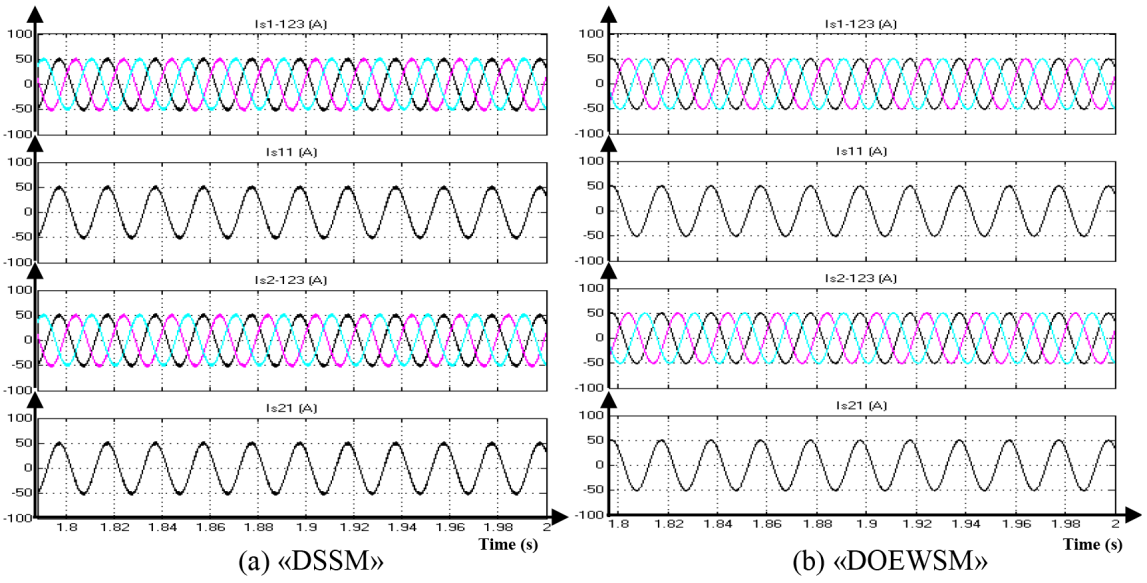

Figure 13. Evolution of the current during the permanent mode.

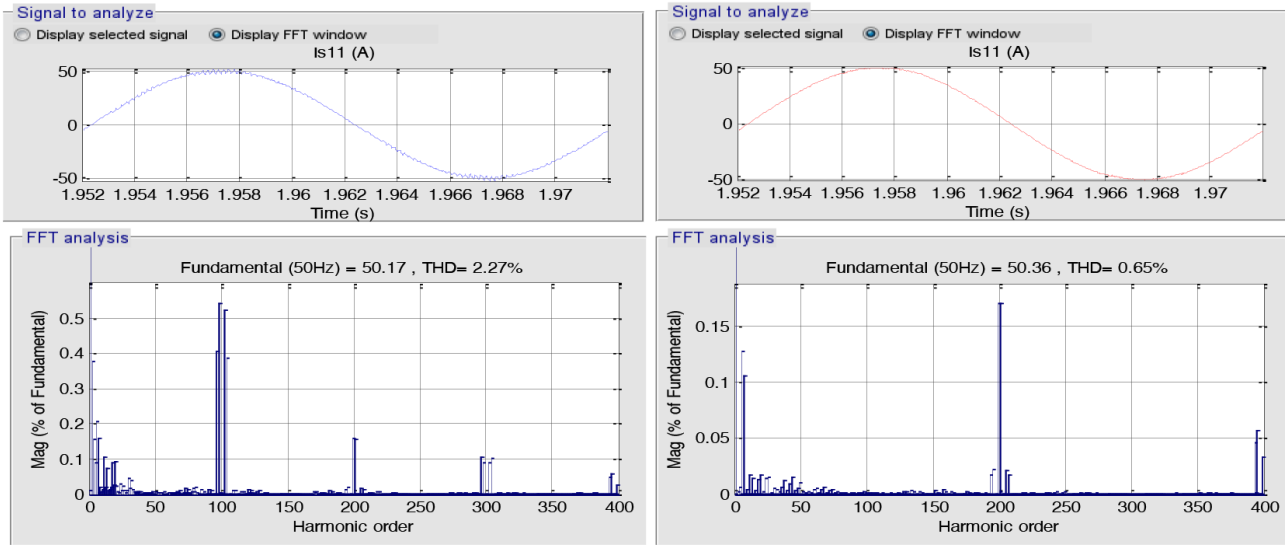

(a) «DSSM» (b) «DOEWSM»

Figure 14. Waveform and harmonic ration of stator current.

The machine "DOEWSM" offers a better THD stator current and extended bandwidth.

The enlarging of the bandwidth shown in Figures 10 and 14 is due to the feeding of the machine by phase opposition voltages, more precisely the PWM strategy in phase opposition used for the control of inverters A1 and A2, even for inverters B1 and B2. To view the influence of the proposed machine with damper windings, we also simulate the same machine without damper windings. Figure 15 shows the simulation results of speed and torque in starting mode when we note the decreases in the undulation of speed and torque for a machine with dampers.

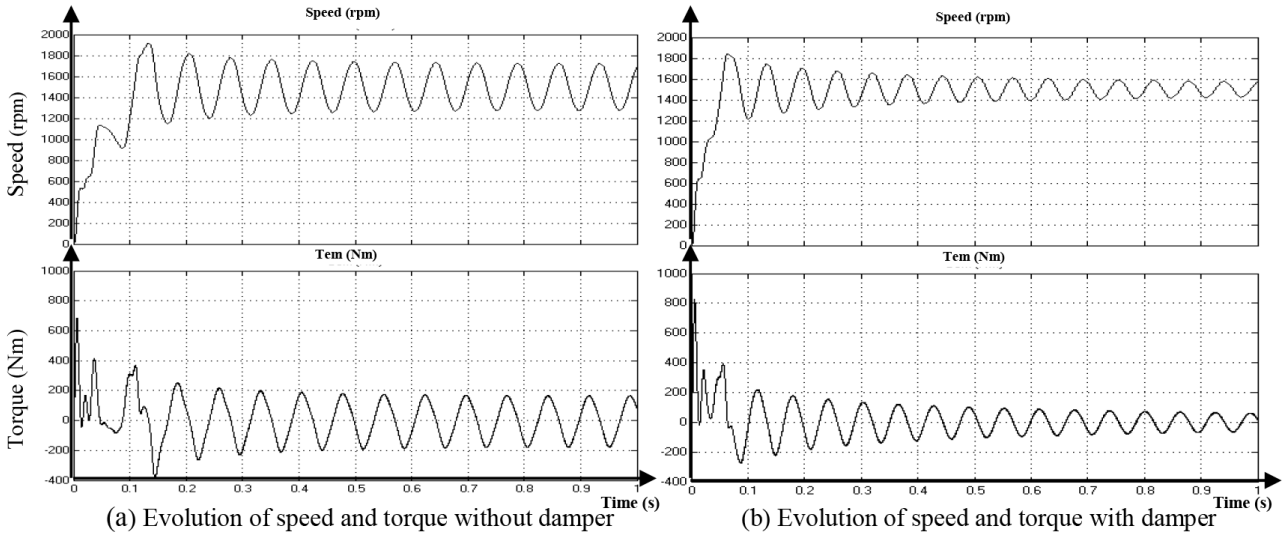

(a) Evolution of speed and torque without damper (b) Evolution of speed and torque with damper

Figure 15. Influence of the dampers for the "DOEWSM".

Table 1 summarizes the THD voltages (%), THD stator current (%), and torque undulation (%) for the two machine structures with P = 40 kW and load torque Tr = 150 Nm. The power inverters for assuring the supply to each machine are also shown in the table.

Table 1. THD voltages (%), undulations of torque (%) and power inverters.

	DSSM	DOEWSM
THD voltage (%)	70.06	44.05
ΔTem (%)	4.8	1.8
THD current (%)	2.27	0.65
Power inverter	P/2	P/4

The different results for THD voltage, THD stator current, and torque undulations show the important advantage of the dual open-end windings synchronous machine.

Furthermore, the novel dual open-end winding synchronous machine is a good solution for power segmentation because of the feeding of this machine by four inverters. Each inverter is dimensioned to a quarter power of the machine.

The characteristics of the synchronous machine are shown in Table 2.

Table 2. The characteristics of the synchronous machine.

Nominal power P	40 kW
Speed n	1500 rpm
Resistance of stator Rs	0.5 Ω
Resistance of wound rotor Rf	0.643 Ω
Resistance of damper Rkd	0.45747 Ω
Resistance of damper Rkq	0.41637 Ω
Inductance of stator Ld	29.85 mH
Inductance of stator Lq	14.87 mH
Inductance of rotor Lf	30.89 mH
Inductance of damper Lkd	30.981 mH
Inductance of damper Lkq	15.882 mH
Mutual inductance of stator 1 and 2 Md	28.89 mH
Mutual inductance of stator 1 and 2 Mq	28.89 mH
Mutual inductance between stator 1, 2, and rotor Mfd	28.89 mH
Mutual inductance between damper axis d and rotor Mfkd	28.89 mH
Mutual inductance between stator 1, 2, and dampers axis d Mkd	28.89 mH
Mutual inductance between stator 1, 2, and dampers axis q Mkq	13.81 mH
Inertia moment J	0.1 kg m^2
Viscous force f	0.001 N.m.s/rad

5. Conclusion

Modeling is presented that describes the operation of a salient-pole wound rotor dual open-end stator winding synchronous machine with damper windings fed by four 2-level inverters based on PWM control strategy.

The simulation results of the dual three-phase open-end winding synchronous machine compared with the double star synchronous machine using THD voltage, THD stator current, and torque undulation allow us to increase the level of machine voltage, give best torque quality, and improve THD voltage and THD stator current of the machine, as well as extend the bandwidth.

This machine structure presents a significant advantage in terms of power segmentation. Indeed, the dimensioning of each inverter is reduced to a quarter power of the machine. This structure requires four transformers with reduced power (P/4). Therefore, this installation is expensive but the association machine with four inverters shows the important advantage for the operation in degraded mode, which increased the liberty degrees of the system. Indeed, the loss of three successive inverters does not stop the machine, which allows us to improve the reliability and availability of the drive system.

References

[1] Stemmler H. High-power industrial drives. Proc IEEE 1994; 82: 1266-1286.

[2] Franquelo LG, Rodriguez J, Leon JI, Kouro S, Portillo R, Prats MAM. The age of multilevel converters arrives. IEEE Ind Electron M 2008; 2: 28-39.

[3] Kouro S, Malinowski M, Gopakumar K, Pou J, Franquelo LG, Wu B, Rodriguez J, Pérez MA, Leon JI. Recent advances and industrial applications of multilevel converters. IEEE T Ind Electron 2010; 57: 2553-2580.

[4] Nabae A, Takahashi I, Akagi H. A new neutral-point-clamped PWM inverter. IEEE T Ind Appl 1981; IA-17.

[5] Meynard TA, Foch H. Multi-level conversion: high voltage choppers and voltage-source inverters. In IEEE 1992 Power Electronics Specialists Conferences, 29 June–3 July 1992; Toledo, OH, USA: IEEE. pp. 397-403.

[6] Lai JS, Peng FZ. Multilevel converters a new breed of power converters. IEEE T Ind Appl 1996; 32: 509-517.

[7] Singh GK, Pant V, Singh YP. Voltage source inverter driven multi-phase induction machine. Elsevier Journal of Computer and Electrical Engineering 2003; 29: 813-834.

[8] Singh GK, Nam K, Lim SK. A simple indirect field-oriented control scheme for multiphase induction machine. IEEE T Ind Electron 2005; 52: 1177-1184.

[9] Jones M, Vukosavic SN, Dujic D, Levi E. A synchronous current control scheme for multiphase induction motor drives. IEEE T Energy Conver 2009; 24: 860-868.

[10] Abdel-Khalik AS, Morsy AS, Ahmed S, Massoud AM. Effect of stator winding connection on performance of five-phase induction machines. IEEE T Ind Electron 2014; 61: 3-19.

[11] Rojoi R, Farina F, Griva G, profumo R, Tenconi A. Direct torque control for dual three-phase induction motors drives. IEEE T Ind Appl 2005; 41: 1627-1636.

[12] Marouani K, Baghli L, Hadiouche D, Kheloui A, Rezzoug A. A new PWM strategy based on a 24-sector vector space decomposition for a six-phase VSI-fed dual stator induction motor. IEEE T Ind Electron 2008; 55: 1910-1920.

[13] Samuli K, Jussi K, Pasi P, Pertti S, Olli P. Determination of the inductance parameters for the decoupled d-q model of double-star permanent-magnet synchronous machines. IET Electr Power App 2014; 8: 39-49.

[14] Guizani S, Ben Ammar F. The eigenvalues analysis of the double star induction machine supplied by redundant voltage source inverter. International Review of Electrical Engineering 2008; 3: 300-311.

[15] Ben Ammar F, Guizani S. The improvement availability of a double star asynchronous machine supplied by redundant voltage source inverter. Journal of Electrical System 2008; 4.

[16] Stemmler H, Geggenbach P. Configurations of high power voltage source inverter drives. Proc EPE Conference 1993; Brighton, UK; 5: 7-12.

[17] Somasekhar VT, Baiju MR, Gopakumar K. Dual two-level inverter scheme for an open-end winding induction motor drive with a single DC power supply and improved DC bus utilization. IEE Proceeding Electric Power Applications 2004; 151: 230-238.

[18] Srinivas S, Somasekhar VT. Space-vector-based PWM switching strategies for a three-level dual-inverter-fed open-end winding induction motor drive and their comparative evaluation. IET Electr Power App 2008; 2: 19-31.

[19] Figarado S, Sivakumar K, Ramchand R, Das A, Patel C, Gopakumar K. Five-level inverter scheme for an open-end winding induction machine with less number of switches. IET Power Electron 2010; 3: 637-647.

[20] Sandulescu AP, Meinguet F, Kestelyn X, Semail E, Bruyere A. Flux-weakening operation of open-end winding drive integrating a cost-effective high-power charger. IET Electrical Systems in Transportation 2013; 3: 10-21.

[21] Bodo N, Levi E, Jones M. Investigation of carrier-based PWM techniques for a five-phase open-end winding drive topology. IEEE T Ind Electron 2013; 60: 2054-2065.

[22] Guizani S, Ben Ammar F. The dual open-end winding induction machine fed by quad inverters in degraded mode. International Journal of Scientific & Engineering Research 2013; 4.

[23] Guizani S, Ben Ammar F. Dual open-end stator winding induction machine fed by redundant voltage source inverters. Turk J Elec Eng & Comp Sci 2015; 23: 2171-2181.